

Synthesis and Rietveld refinements of new ceramics $\text{Sr}_2\text{CaFe}_2\text{WO}_9$ and $\text{Sr}_2\text{PbFe}_2\text{TeO}_9$ perovskites

Abdelhadi El Hachmi,¹ Y. Tamraoui,^{1,2} Bouchaib Manoun,^{1,2,a)} R. Haloui,¹ M.A. Elaamrani,¹ I. Saadouné,^{2,3} L. Bih,⁴ and P. Lazor⁵

¹Univ Hassan Ier, Laboratoire des Sciences des Matériaux, des Milieux et de la modélisation (LS3M), 25000 Khouribga, Morocco

²Materials Science and nano-engineering (MSN), University Mohammed VI Polytechnic, Lot 660 Hay Moulay Rachid, 43150 Ben Guerir, Morocco

³LCME, FST Marrakech, University Cadi Ayyad, Av. A. Khattabi, 40000 Marrakech, Morocco

⁴Equipe de Physico-Chimie de la Matière Condensée, PCMC, Faculté des Sciences de Meknès, Université Moulay Ismail, Morocco

⁵Department of Earth Sciences, Uppsala University, SE-752 36, Uppsala, Sweden

(Received 18 October 2017; accepted 21 January 2018)

Ceramics of $\text{Sr}_2\text{CaFe}_2\text{WO}_9$ and $\text{Sr}_2\text{PbFe}_2\text{TeO}_9$ double perovskites have been prepared in polycrystalline form by solid-state technique, in the air. The crystalline structure was analyzed using X-ray powder diffraction (XRPD) at room temperature. Rietveld analysis of XRPD patterns show that both compounds adopt a tetragonal structure with space group $I4/m$, with unit cell parameters $a = 5.5453(1)$ Å, $c = 7.8389(1)$ Å for $\text{Sr}_2\text{CaFe}_2\text{WO}_9$, and $a = 5.5994(15)$ Å, $c = 7.8979(30)$ Å for $\text{Sr}_2\text{PbFe}_2\text{TeO}_9$. A certain degree of anti-site disordering of W and/or Te and Fe on the B –sites have been detected, indicating the presence of a partial amount of W and/or Te at Fe positions and vice versa. © 2018 International Centre for Diffraction Data. [doi:10.1017/S0885715618000222]

Key words: $\text{Sr}_2\text{CaFe}_2\text{WO}_9$, $\text{Sr}_2\text{PbFe}_2\text{TeO}_9$ crystal structure, X-ray diffraction

I. INTRODUCTION

Multiferroic oxides materials have combined electric, magnetic, and/or structural order parameters that result in simultaneous ferromagnetic, ferroelectric, and/or ferroelastic behaviors. The discovery of colossal magnetoresistance (CMR) in an ordered structure Sr_2FeMO_6 ($M = \text{Mo}, \text{W}$) has resulted in many recent research in double perovskite oxides with general formula $\text{A}_2\text{BB}'\text{O}_6$ (Kobayashi *et al.*, 1998; Dass and Goodenough, 2001; García-Hernández *et al.*, 2001; Ray *et al.*, 2001; Branford *et al.*, 2003; Philipp *et al.*, 2003; Sher and Atfield, 2006; Dhahri *et al.*, 2009; Gong *et al.*, 2014). The ordering of Fe and Mo or W cations in the octahedral B-sites in the cubic high-symmetry structure double perovskite lattice leads to ferrimagnetism with a high Curie temperature (T_C) of ≈ 420 K for $\text{Sr}_2\text{FeMoO}_6$ (Kobayashi *et al.*, 1998), while for Sr_2FeWO_6 it is known to be antiferromagnetic insulator with $T_N \approx 37$ K (Kawanaka *et al.*, 2000), it has contrasting transport properties.

Low-field magneto-resistance emerges from spin-dependent electrons transfer to grain or magnetic domain confines. This property, related to the variation of electric resistivity when a magnetic field is applied, is a consequence of the half-metallic character of the double perovskite (Philipp *et al.*, 2003). Early, the CMR materials of perovskite oxides have prospects of great opportunities for the development of new technologies, potentially applied including nonvolatile magnetic random access memory, magnetic read/write heads for hard drives, magnetic tunnel junction, and other magnetic sensor applications. Among the explored analogues of Sr_2FeMO_6 ($M = \text{Mo}, \text{W}$), it

was reported that A_2CrMoO_6 ($A = \text{Sr}, \text{Ba}$) (Arulraj *et al.*, 2000; Sher and Atfield, 2006) is also a ferrimagnet with a high Curie temperature of ≈ 450 K (Arulraj *et al.*, 2000). The partial disorder of Cr and Mo in the B-sites of double perovskite offers an important role in the structural, electrical and magnetic properties of these compounds (Arulraj *et al.*, 2000; Sher and Atfield, 2006).

As mentioned the disorder in the B-site has an important role in the behavior of physical properties. Extensive studies have been conducted to ameliorate, and/or explain this antisite-disorder and its effects on the properties, by the way of synthesis procedures or theoretical calculation (density functional theory: DFT) and the structural identification by means of Rietveld refinement. Also using magnetic measurements as a sensitive tool to demonstrate the antisite-disorder and to understand the ferromagnetic, magnetic and magneto-electric behavior (Sánchez *et al.*, 2002; Ivanov *et al.*, 2007).

As the synthesis of Sr_2AlMO_6 ($M = \text{Nb}, \text{Ta}$) double perovskite (Woodward *et al.*, 1994) which have been prepared by several different methods shows that the order degrees of octahedral site cations are obtained depending on the synthesis conditions. The series of $\text{Ni}_{1-x}\text{Co}_x\text{Cr}_2\text{O}_4$ spinels were also reported as antisite-disordered compound with optical and magnetic properties (GAO *et al.*, 2017). Some of the A sites are occupied by Cr^{+3} ions and some of the B sites are occupied by Ni and Co cations. This departure from the normal spinel structure causes the antisite defect. These antisite defects play an important role in ions surface interaction process and influence the electrical and optical behaviors. The antisite-disorder was also observed in several triple perovskites, such as $\text{Sr}_3\text{Fe}_2\text{TeO}_9$ (S space group $I4/m$), $\text{Ba}_3\text{Fe}_2\text{TeO}_9$ (space group $P6_3/mmc$) (Ivanov *et al.*, 2007; Tang *et al.*, 2016), $\text{Ca}_3\text{Fe}_2\text{WO}_9$ (space group $I4/m$) (Ivanov *et al.*, 2005), $\text{Sr}_3\text{Fe}_2\text{MoO}_9$ (space group $I4/m$), $\text{Sr}_3\text{Fe}_2\text{WO}_9$ (space group

^{a)}Author to whom correspondence should be addressed. Electronic mail: manounb@gmail.com

$I4/m$), $\text{Sr}_3\text{Fe}_2\text{WO}_9$ (space group $I4/m$) (Viola *et al.*, 2003), $\text{Ba}_{1.6}\text{Sr}_{1.4}\text{Fe}_2\text{WO}_9$ (space group $P6_3/mmc$) (Manoun *et al.*, 2011). Recently perovskite series $\text{Sr}_{3-x}\text{Ca}_x\text{Fe}_2\text{TeO}_9$ ($0 \leq x \leq 1$) (El Hachmi *et al.*, 2017) were reported by our research team showing that the antisite-disorder is affected with increasing the Calcium amount from $x = 0$ to $x = 1$.

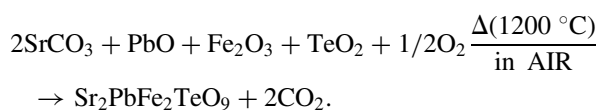
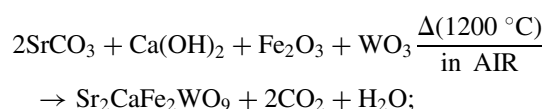
Using solid state reaction as synthesis technique, two perovskite compounds Ca^{+2} and Pb^{+2} doped $\text{Sr}_3\text{Fe}_2\text{WO}_9$, and $\text{Sr}_3\text{Fe}_2\text{TeO}_9$ respectively, are reported in this work with general formula $\text{Sr}_2\text{CaFe}_2\text{WO}_9$ and $\text{Sr}_2\text{PbFe}_2\text{TeO}_9$. Using X-ray powder diffraction (XRPD) the compounds are easily identified to adopt the perovskite structure. The refined crystal structure was reported and the antisite-disorder in the B and B' sites was discussed.

II. EXPERIMENTAL

A. Synthesis

Polycrystalline powders of $\text{Sr}_2\text{CaFe}_2\text{WO}_9$ and $\text{Sr}_2\text{PbFe}_2\text{TeO}_9$ were synthesized using the standard solid-state reaction from stoichiometric mixtures of SrCO_3 (99.995%), $\text{Ca}(\text{OH})_2$ (99.995%), Fe_2O_3 ($\geq 99.98\%$), WO_3 (99.9%), PbO (99.99%), and TeO_2 (99.99%), all received from Sigma–Aldrich. The mixtures were ground in an agate mortar then heated progressively to 650 and 900 °C for 18 h, in alumina crucibles. The resulting powders were reground and calcined at 1200 °C for 24 h in air. The samples were cooled to room temperature for re-grinding and sintering several times to improve the homogeneity.

The chemical reactions are:



B. X-ray powder diffraction

Diffraction data were collected at room temperature on a D2 PHASER diffractometer, with the Bragg–Brentano geometry, using $\text{Cu } K_\alpha$ radiation ($\lambda = 1.5418 \text{ \AA}$) with 30 KV and 10 mA, Soller slits of 0.02 rad on incident and diffracted beams; divergence slit of 0.5°; antiscatter slit of 1°; receiving slit of 0.1 mm; with sample spinner, and a Lynxeye detector type with a maximum global count rate >1000000000 cps. The pattern was scanned through steps of 0.010142° (2θ), between 15 and 105° (2θ) with a fixed-time counting of 2 s/step.

The WinPlotr software (Roisnel and Rodríguez-Carvajal, 2001), integrated in the FullProf program (Rodríguez-Carvajal, 1990) was used to refine the crystal structure by the Rietveld method. The peak shape was described by a pseudo-Voigt function and the background level was modeled using a polynomial function.

The following structural and instrumental parameters were refined from the XRD data: scale factor, background coefficients, zero-point error, unit-cell parameters, pseudo-Voigt corrected for asymmetry parameters, Caglioti parameters (U, V, and W), atomic positions, an overall isotropic thermal factor,

and antisite disorder of Fe/W and Fe/Te. The starting data needed for Rietveld refinements are the atomic positions and unit cell parameters, the model was taken from the previous studies (Ivanov *et al.*, 2001; Viola *et al.*, 2005).

III. RESULTS AND DISCUSSION

A. Structure determination and description of the structure

At room temperature the XRPD patterns of the compounds, with nominal compositions, $\text{Sr}_2\text{CaFe}_2\text{WO}_9$ and $\text{Sr}_2\text{PbFe}_2\text{TeO}_9$ are easily identified to adopt the perovskite structure (Figure 1) and by means of the computer program Dicvol (Boultif *et al.*, 1991) using the first 15 peak position with a maximal error of 0.03° as input data. The XRPD patterns were assigned to a tetragonal symmetry with $I4/m$ as a space group for both compositions.

Figure 1 presents the superposition of the XRPD patterns at room temperature of $\text{Sr}_2\text{CaFe}_2\text{WO}_9$ and $\text{Sr}_2\text{PbFe}_2\text{TeO}_9$. Bragg positions (2θ) of the peaks are shifted slightly to lower angles when we replace tungsten and calcium by tellurium and lead atoms respectively, this is may be due to electronic configuration effects and the ionic radii of those cations. The ionic radii of W^{6+} and Te^{6+} are 0.6 and 0.56 Å, respectively, and for Ca^{2+} and Pb^{2+} are 1.34 and 1.49 Å (Shannon, 1976). The XRPD patterns of the $\text{Sr}_2\text{CaFe}_2\text{WO}_9$ and $\text{Sr}_2\text{PbFe}_2\text{TeO}_9$ double perovskites were refined by Rietveld method (Rietveld, 1969). The details of Rietveld refinements such as lattice parameters, cell volumes, and reliability factors are given in Table I.

The structural refinement of $\text{Sr}_2\text{CaFe}_2\text{WO}_9$ and $\text{Sr}_2\text{PbFe}_2\text{TeO}_9$ taken at room temperature from XRPD data were performed in a tetragonal system with space group $I4/m$ (ITA- No.87). Impurity corresponding to scheelite structure, SrWO_4 (ICDD# 01-085-0587) was included in the refinement as the second phase with space group $I4_1/a$ (ITA-No.88) for $\text{Sr}_2\text{CaFe}_2\text{WO}_9$. The percentage of this impurity is about 3.7%, according to the Rietveld refinements.

The Rietveld refinement results show that Sr, (Ca or Pb) atoms were located at the 4d (0,1/2,1/4) positions of S_4 symmetry, Fe(1)/M(1) at 2a (0,0,0) and Fe(2)/M(2) at 2b (00,1/2) sites of C_{4h} symmetry ($M = \text{W, Te}$), and oxygen atoms at the 8 h (x,y,0) and 4e (0,0,z) positions (C_s and C_4

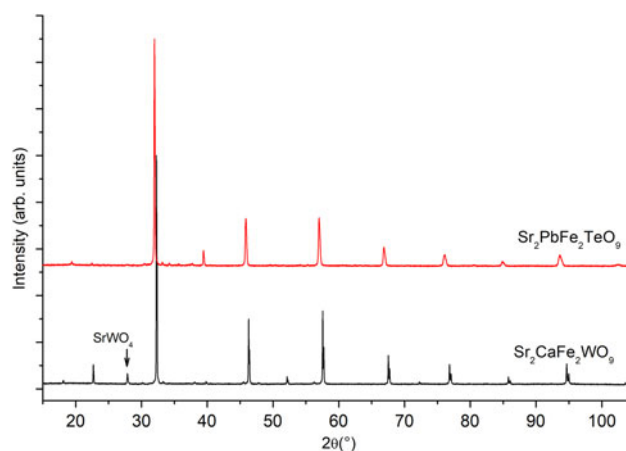


Figure 1. (Colour online) X-ray powder diffraction patterns of ceramics $\text{Sr}_2\text{CaFe}_2\text{WO}_9$ and $\text{Sr}_2\text{PbFe}_2\text{TeO}_9$ taken at room temperature.

TABLE I. Details of Rietveld refinement for Sr₂CaFe₂WO₉ and Sr₂PbFe₂TeO₉ double perovskites at 298 K.

Composition	Sr ₂ CaFe ₂ WO ₉	Sr ₂ PbFe ₂ TeO ₉
Wavelength (Å)	$\lambda_{k\alpha 1} = 1.54056,$ $\lambda_{k\alpha 2} = 1.54439$	$\lambda_{k\alpha 1} = 1.54056$ $\lambda_{k\alpha 2} = 1.54439$
2 θ step scan increment (°)	0.010142	0.010142
2 θ range (°)	15.002–104.997	15.002–104.997
Program	FullProf	FullProf
Zero-point (2 θ °)	0.0218 (7)	−0.0188 (18)
Pseudo-Voigt function	$\eta = 0.49$ (2)	$\eta = 0.6993$ (8)
PV = $\eta L + (1 - \eta) G$		
Caglioti parameters	$U = 0.0076$ (8) $V = -0.00219$ (80) $W = 0.0044$ (2)	$U = 0.1616$ (1) $V = -0.0541$ (1) $W = 0.0123$ (3)
No. of reflections	155/2	172/2
No. of refined parameter	33	24
crystal system	Tetragonal	Tetragonal
Space group	<i>I4/m</i>	<i>I4/m</i>
a (Å)	5.5453 (7)	5.5994 (15)
c (Å)	7.8389 (1)	7.8979 (30)
V (Å ³)	241.05 (1)	247.224 (13)
Z	4	4
Atom number	5	5
R _B	3.02	4.89
R _F	7.56	8.09
R _p	3.53	3.32
R _{wp}	4.9	4.46
cR _p	3.52	3.21
cR _{wp}	4.94	4.28
χ^2	1.93	1.41

symmetries, respectively). The two Fe³⁺ and M⁶⁺ cations were found to occupy alternatively two sites; 2a and 2b with different amounts even if there are differences between the sizes and valence charges of these cations. The combination between Fe³⁺ and W⁶⁺ or Te⁶⁺ cations generally favors disordered arrangement in Sr₂CaFe₂WO₉ and Sr₂PbFe₂TeO₉. Structural details at room temperature such as atomic positions, isotropic displacement parameters, occupancy, and site symmetry are given in Table II. The Crystallographic Information Frameworks (CIF) files are available in the supplementary material.

The Fe/M (*M* = W or Te) arrangement over the two crystallographically distinct B-sites was allowed to vary, with the constraint that the 2 : 1 composition ratio was maintained. From the structural refinement of these both compounds, an anti-site disordering effect was detected, we noted that in Sr₂CaFe₂WO₉ some W⁶⁺ from the 2b positions randomly

replace some Fe³⁺ at 2a positions; 2b-sites are predominantly occupied by Fe³⁺ atoms compared with W⁶⁺. Again, in Sr₂PbFe₂TeO₉, some Te⁶⁺ from the 2a positions randomly replace some Fe at 2b positions; 2b-sites are predominantly occupied by Fe³⁺ atoms compared with Te⁶⁺. The thermal factors for (2a and 2b) positions in the space group *I4/m* were constrained.

The goodness of fit is illustrated in Figures 2 and 3, showing an excellent agreement between observed and calculated XRPD patterns. The reliability factors and χ^2 , giving different measures of the quality of fits, are small and indicate a good quality of refinements Table I.

According to the crystallographic data obtained from Rietveld refinements of stoichiometric compounds Sr₂CaFe₂WO₉ and Sr₂PbFe₂TeO₉, Fe and W or Te cations are octahedrally coordinated with the oxygen atoms. The (Fe/W)O₆/(Fe/Te)O₆ octahedra are alternately connected and extended in three dimensions. Generally, the ionic sizes or electronic effects of Fe³⁺, Te⁶⁺, and W⁶⁺ cations have influences on the octahedral tilt angles and the associated bond angles. At room temperature, the selected bond lengths (Å) and angles (°) are listed in Table III.

Structural views of Sr₂CaFe₂WO₉ and Sr₂PbFe₂TeO₉ is made up of alternate corner shared octahedra, i.e., (Fe/M)_{2a}O₆ and (Fe/M)_{2b}O₆ (*M* = W or Te). Along the *c*-axis, these octahedra are connected through oxygen atoms O(2); and in the *ab*-plane, they are connected by O(1) atoms. Due to the special positions occupied by the Fe and W or Te atoms at both 2a and 2b-sites, and oxygen atoms O(2) at 4e-sites, along the *c*-axis the bond angle of (Fe/M)_{2a}–O(2)–(Fe/M)_{2b} is constrained to be 180°. The (Fe/M)_{2a}O₆ and (Fe/M)_{2b}O₆ octahedra are ordered and alternate along the three directions, in a way that each (Fe/M)_{2a}O₆ octahedron is linked via corners to six (Fe/M)_{2b}O₆ octahedra and vice versa. The unit cell parameters were refined (Table I) with the complete powder diffraction data set (Tables IV and V). Intensities given in Tables IV and V are obtained from the “observed intensities” of the Rietveld refinement.

For Sr₂CaFe₂WO₉ a drawing of the anti-phase tilting of the structure is shown in Figure 4; it contains alternating (Fe/W)_{2a}O₆ and (Fe/W)_{2b}O₆ octahedra, exhibiting a tilting angle of $\psi_{001} = 6.85^\circ$ and tilted in anti-phase in the basal *ab*-plane (along the [001] direction) of the pseudo-cubic cell. This corresponds to the [a⁰a⁰c[−]] Glazer notation (Glazer, 1975) as derived by Woodward (1997 for 1 : 1 ordering of double perovskites, consistent with space group *I4/m*. The calculated (Fe/W)_{2a}–O(1)–(Fe/W)_{2b} bond angle is 164.0(2)°. The (Fe/W)_{2a}O₆ octahedra exhibit an average

TABLE II. Positional and thermal parameters for ceramics Sr₂CaFe₂WO₉ and Sr₂PbFe₂TeO₉ after a Rietveld refinement XRPD data collected at 298 K.

Atom	Wyckoff site	x	y	z	B _{iso} (Å ²)	occ.	Site symmetry
Sr ₂ CaFe ₂ WO ₉							
Sr/Ca	4d	0	1/2	1/4	1.17 (6)	0.667/0.333	−4.
Fe(1)/W(1)	2a	0	0	0	0.23 (5)	0.640/0.360	4/m.
W(2)/Fe(2)	2b	0	0	1/2	0.23 (5)	0.310/0.690	4/m.
O1	8 h	0.282 (7)	0.212 (12)	0	2.2 (3)	1	m.
O2	4e	0	0	0.258 (9)	2.2 (3)	1	4.
Sr ₂ PbFe ₂ TeO ₉							
Sr/Pb	4d	0	1/2	1/4	3.949 (7)	0.667/0.333	−4.
Fe(1)/Te(1)	2a	0	0	0	0.072 (2)	0.515/0.485	4/m.
Te(2)/Fe(2)	2b	0	0	1/2	0.072 (2)	0.181/0.819	4/m.
O1	8 h	0.275(4)	0.211(6)	0	0.954 (3)	1	m.
O2	4e	0	0	0.242(7)	0.954 (3)	1	4.

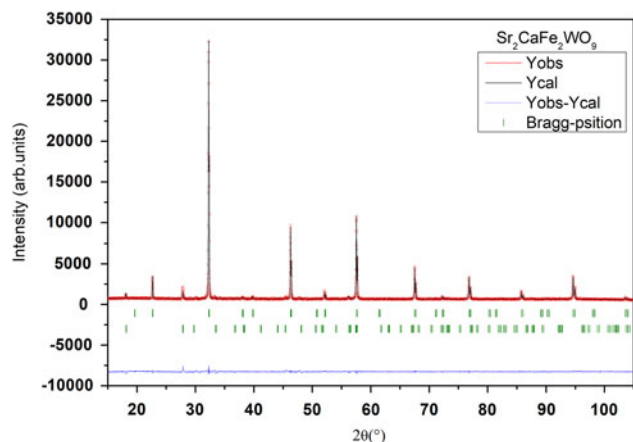


Figure 2. (Colour online) Final Rietveld plots for compound $\text{Sr}_2\text{CaFe}_2\text{WO}_9$. The upper symbols illustrate the observed data (circles) and the calculated pattern (solid line). The vertical markers show calculated positions of Bragg reflections. The lower curve is the difference diagram. The second series of tick marks corresponds to the Bragg reflections of a minor impurity of SrWO_4 .

$(\text{Fe}/\text{W})_{2a}\text{-O}$ bond length of $1.98(2)$ Å, slightly larger than the $(\text{Fe}/\text{W})_{2b}\text{-O}_6$ octahedra; with an average $(\text{Fe}/\text{W})_{2b}\text{-O}$ bond length of $1.968(3)$ Å. Along c -axis, the observed octahedra at the 2a-sites are elongated, whereas the observed octahedra at 2b-sites are significantly flattened, as shown in Table III.

The ionic distribution of Fe^{3+} and W^{6+} cations in $\text{Sr}_2\text{CaFe}_2\text{WO}_9$ may be re-written by the formula: $[\text{Sr}_2\text{Ca}]_{4d}[\text{Fe}_{0.962(4)}\text{W}_{0.538(4)}]_{2a}[\text{Fe}_{1.038(4)}\text{W}_{0.462(4)}]_{2b}\text{O}_9$, with the $\text{Fe}^{3+}/\text{W}^{6+}$ cations at the 2a-site are surrounded by six 2b-sites, which are occupied on average of 64% by Fe^{3+} and 36% by W^{6+} ions. Vice-versa, $\text{Fe}^{3+}/\text{W}^{6+}$ cations at 2b-sites are surrounded by six 2a-sites, which are occupied on average 69% by Fe^{3+} ions and 31% by W^{6+} ions.

For $\text{Sr}_2\text{PbFe}_2\text{TeO}_9$ a drawing of the anti-phase tilting of the structure is illustrated in Figure 5; it contains alternating $(\text{Fe}/\text{Te})_{2a}\text{O}_6$ and $(\text{Fe}/\text{Te})_{2b}\text{O}_6$ octahedra, presenting a tilting angle of $\psi_{001} = 7.3^\circ$ and tilted in anti-phase in the basal ab -plane (along the $[001]$ direction) of the pseudocubic cell. This corresponds to the $[a^0a^0c^-]$ Glazer notation (Glazer, 1975) as derived by Woodward (1997) for 1 : 1 ordering of double perovskites, consistent with space group $I4/m$. The calculated $(\text{Fe}/\text{Te})_{2a}\text{-O}(1)\text{-}(\text{Fe}/\text{Te})_{2b}$ bond angle is $165.4(11)^\circ$.

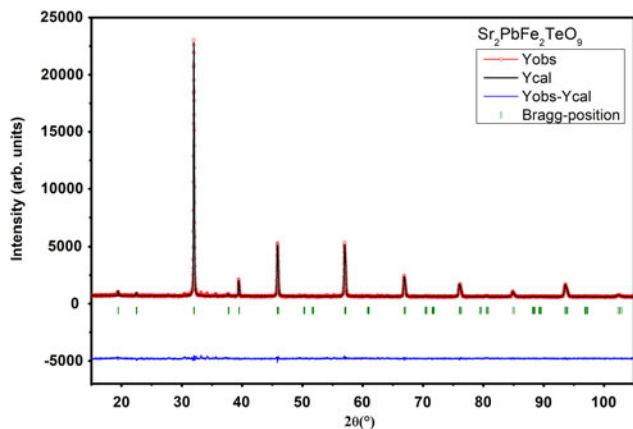


Figure 3. (Colour online) Final Rietveld plots for compound $\text{Sr}_2\text{PbFe}_2\text{TeO}_9$. The upper symbols illustrate the observed data (circles) and the calculated pattern (solid line). The vertical markers show calculated positions of Bragg reflections. The lower curve is the difference diagram.

TABLE III. Selected bond lengths (Å) and angles ($^\circ$) for $\text{Sr}_2\text{CaFe}_2\text{WO}_9$ and $\text{Sr}_2\text{PbFe}_2\text{TeO}_9$ at room temperature calculated from XRPD pattern with $I4/m$ space group.

$\text{Sr}_2\text{CaFe}_2\text{WO}_9$		$\text{Sr}_2\text{PbFe}_2\text{TeO}_9$	
$4 \times (\text{Sr}/\text{Ca})_{4d}\text{-O1}$	2.97 (2)	$4 \times (\text{Sr}/\text{Pb})_{4d}\text{-O1}$	2.98 (2)
$4 \times (\text{Sr}/\text{Ca})_{4d}\text{-O1}$	2.59 (1)	$4 \times (\text{Sr}/\text{Pb})_{4d}\text{-O1}$	2.622 (2)
$4 \times (\text{Sr}/\text{Ca})_{4d}\text{-O2}$	2.77 (1)	$4 \times (\text{Sr}/\text{Pb})_{4d}\text{-O2}$	2.798 (1)
$\langle (\text{Sr}/\text{Ca})_{4d}\text{-O} \rangle$	2.78 (1)	$\langle (\text{Sr}/\text{Pb})_{4d}\text{-O} \rangle$	2.80 (1)
$4 \times (\text{Fe}/\text{W})_{2a}\text{-O1}$	1.96 (1)	$4 \times (\text{Fe}/\text{Te})_{2a}\text{-O1}$	1.94 (2)
$2 \times (\text{Fe}/\text{W})_{2a}\text{-O2}$	2.02 (2)	$2 \times (\text{Fe}/\text{Te})_{2a}\text{-O2}$	1.91 (6)
$\langle (\text{Fe}/\text{W})_{2a}\text{-O} \rangle$	1.98 (2)	$\langle (\text{Fe}/\text{Te})_{2a}\text{-O} \rangle$	1.93 (1)
$4 \times (\text{Fe}/\text{W})_{2b}\text{-O1}$	2.003 (1)	$4 \times (\text{Fe}/\text{Te})_{2b}\text{-O1}$	2.05 (3)
$2 \times (\text{Fe}/\text{W})_{2b}\text{-O2}$	1.897 (3)	$4 \times (\text{Fe}/\text{Te})_{2b}\text{-O2}$	2.04 (6)
$\langle (\text{Fe}/\text{W})_{2b}\text{-O} \rangle$	1.968 (3)	$\langle (\text{Fe}/\text{Te})_{2b}\text{-O} \rangle$	2.05 (4)
$4 \times ((\text{Fe}/\text{W})_{2a}\text{-O1} - (\text{Fe}/\text{W})_{2b})$	164.0 (2)	$4 \times ((\text{Fe}/\text{Te})_{2a}\text{-O1} - (\text{Fe}/\text{Te})_{2b})$	165.4 (11)
$4 \times ((\text{Fe}/\text{W})_{2a}\text{-O2} - (\text{Fe}/\text{W})_{2b})$	180	$4 \times ((\text{Fe}/\text{Te})_{2a}\text{-O2} - (\text{Fe}/\text{Te})_{2b})$	180

The $(\text{Fe}/\text{Te})_{2a}\text{O}_6$ octahedra exhibit an average $(\text{Fe}/\text{Te})_{2a}\text{-O}$ bond length of $1.93(2)$ Å, shorter than the $(\text{Fe}/\text{Te})_{2b}\text{O}_6$ octahedra; with an average $(\text{Fe}/\text{Te})_{2b}\text{-O}$ bond length of $2.05(3)$ Å. Through c -axis, the observed octahedra at the 2b-sites are elongated, whereas the observed octahedra at 2a-sites are significantly compressed, as displayed in Table III.

The ionic distribution of Fe^{3+} and Te^{6+} cations in $\text{Sr}_2\text{PbFe}_2\text{TeO}_9$ perhaps re-written by the formula: $[\text{Sr}_2\text{Pb}]_{4d}[\text{Fe}_{0.772(2)}\text{Te}_{0.728(2)}]_{2a}[\text{Fe}_{1.228(2)}\text{Te}_{0.272(2)}]_{2b}\text{O}_9$, with the $\text{Fe}^{3+}/\text{Te}^{6+}$ cations at the 2a-site are surrounded by six 2b-sites, which are occupied on average 51.5% by Fe^{3+} and 48.5% by Te^{6+} ions. $\text{Fe}^{3+}/\text{Te}^{6+}$ cations at 2b-site are surrounded by six 2a-sites, which are occupied on average 81.9% by Fe^{3+} ions and 18.1% by Te^{6+} ions.

In fact, the average $(\text{Fe}/\text{M})\text{-O}$ bond lengths obtained from Rietveld refinements of the compounds $\text{Sr}_2\text{CaFe}_2\text{WO}_9$ and $\text{Sr}_2\text{PbFe}_2\text{TeO}_9$ are very similar to those found in other oxides with Fe^{3+} and W^{6+} or Te^{6+} cations (Ivanov *et al.*, 2001; Viola *et al.*, 2005; Manoun *et al.*, 2011) and in agreement with the individual Fe^{3+} , W^{6+} , $\text{Te}^{6+}\text{-O}$ bond length calculated from Shannon's ionic radii ($\text{Fe-O} = 2.065$ Å, $\text{W-O} = 2.02$ Å and $\text{Te-O} = 1.96$ Å) for high-spin electron configuration in octahedral coordination (Shannon, 1976).

Antisite-disorder of Fe^{3+} and W^{6+} or Te^{6+} cations on B and B' sites in the perovskite structure with general formula $\text{A}_3\text{B}_2\text{B}'\text{O}_9$ or $\text{A}_2\text{BB}'\text{O}_6$, has a direct effect on the physical properties (Baum *et al.*, 2004; Ivanov *et al.*, 2004; Pinacca *et al.*, 2005). In our case the ordering of iron and tungsten/tellurium cations is located in 2a and 2b sites of the tetragonal structure ($I4/m$). The formula, for $\text{Sr}_2\text{CaFe}_2\text{WO}_9$, can be written as: $[\text{Sr}_2\text{Ca}]_{4d}[\text{Fe}_{0.962(4)}\text{W}_{0.538(4)}]_{2a}[\text{Fe}_{1.038(4)}\text{W}_{0.462(4)}]_{2b}\text{O}_9$ or $[\text{Sr}_{0.667}\text{Ca}_{0.333}]_{4d}[\text{Fe}_{0.641}\text{W}_{0.359}]_{2a}[\text{Fe}_{0.69}\text{W}_{0.31}]_{2b}\text{O}_6$, and for $\text{Sr}_2\text{PbFe}_2\text{TeO}_9$ it can be written as $[\text{Sr}_2\text{Pb}]_{4d}[\text{Fe}_{0.772(2)}\text{Te}_{0.728(2)}]_{2a}[\text{Fe}_{1.228(2)}\text{Te}_{0.272(2)}]_{2b}\text{O}_9$ or $[\text{Sr}_{0.667}\text{Pb}_{0.333}]_{4d}[\text{Fe}_{0.515}\text{Te}_{0.485}]_{2a}[\text{Fe}_{0.819}\text{Te}_{0.181}]_{2b}\text{O}_6$.

Previously Ivanov *et al.* (2007), reported on the magneto-electric perovskite $\text{Sr}_3\text{Fe}_2\text{TeO}_9$ using magnetic measurements and neutron powder diffraction, it was shown that the antisite-disorder behavior has a direct effect on the magnetic property. Correlation between the structural and magnetic properties was also reported, the magnetic temperature transition (T_N) is strongly related to the value of the $\text{Fe}^{3+}\text{-O-Te}^{6+}$ angle and with lattice distortions. Similar works are also reported

TABLE IV. Powder diffraction data of Sr₂CaFe₂WO₉ (Cu K α ; $\lambda = 1.54056 \text{ \AA}$).

$2\theta_{\text{obs}}$ [°]	$2\theta_{\text{cal}}$ [°]	$\Delta(2\theta)$ [°]	hkl	d_{obs} [Å]	d_{cal} [Å]	$\Delta(d)$ [Å]	I_{obs}/I_0 [%]	I_{cal}/I_0 [%]
19.5940	19.593	-0.0010	011	4.5268	4.5270	0.0002	<1	<1
22.6866	22.658	-0.0286	110	3.9162	3.9211	0.0049	7	7
32.2865	32.259	-0.0275	020	2.7703	2.7726	0.0023	100	43
	32.267	-0.0195	112		2.7720	0.0017		100
39.8117	39.790	-0.0217	022	2.2623	2.2635	0.0012	1	2
46.2979	46.269	-0.0289	220	1.9593	1.9605	0.0012	28	28
	46.290	-0.0079	004		1.9597	0.0003		19
57.5570	57.530	-0.0271	132	1.5999	1.6006	0.0007	17	17
	57.544	-0.0131	024		1.6003	0.0003		20
67.5404	67.508	-0.0324	040	1.3857	1.3863	0.0006	7	7
	67.524	-0.0164	224		1.3860	0.0003		17
72.2448	72.219	-0.0258	330	1.3066	1.3070	0.0004	<1	<1
	72.223	-0.0218	042		1.3069	0.0003		<1
	72.235	-0.0098	134		1.3067	0.0001		1
	72.256	0.0112	006		1.3064	-0.0002		<1
76.8428	76.809	-0.0339	240	1.2395	1.2399	0.0005	3	3
	76.813	-0.0299	332		1.2399	0.0004		6
	76.845	0.0021	116		1.2394	-0.0000		8
85.7990	85.781	-0.0181	044	1.1315	1.1317	0.0002	7	7
94.6598	94.622	-0.0378	152	1.0476	1.0479	0.0003	4	4
	94.634	-0.0258	244		1.0478	0.0002		4
	94.653	-0.0068	316		1.0476	0.0001		4
103.6337	103.585	-0.0487	440	0.9799	0.9802	0.0003	1	2
	103.648	0.0143	008		0.9798	-0.0001		1

TABLE V. Powder diffraction data of Sr₂PbFe₂TeO₉ (Cu K α ; $\lambda = 1.54056 \text{ \AA}$).

$2\theta_{\text{obs}}$ [°]	$2\theta_{\text{cal}}$ [°]	$\Delta(2\theta)$ [°]	hkl	d_{obs} [Å]	d_{cal} [Å]	$\Delta(d)$ [Å]	I_{obs}/I_0 [%]	I_{cal}/I_0 [%]
19.3712	19.427	0.0558	011	4.5784	4.5654	-0.013	4	2
22.4248	22.455	0.0302	110	3.9615	3.9561	-0.0054	0	1
	22.496	0.0712	002		3.9490	-0.0125		0
31.9751	31.966	-0.0091	020	2.7967	2.7974	0.0007	100	100
	31.996	0.0209	112		2.7949	-0.0018		53
39.4278	39.442	0.0142	022	2.2835	2.2827	-0.0008	10	11
45.8711	45.835	-0.0361	220	1.9766	1.9781	0.0015	31	33
	45.923	0.0519	004		1.9745	-0.0021		17
56.9965	56.989	-0.0075	132	1.6144	1.6146	0.0002	9	9
	57.045	0.0485	024		1.6131	-0.0013		18
66.8755	66.831	-0.0445	040	1.3979	1.3987	0.0008	8	8
	66.900	0.0245	224		1.3974	-0.0005		17
76.0091	76.007	0.0021	240	1.2511	1.2510	-0.0001	4	4
76.0647	76.023	0.0417	332	1.2503	1.2508	0.0005	6	6
76.3159	76.377	0.0611	116	1.2468	1.2490	-0.0022	2	3
84.8830	84.890	0.007	044	1.1415	1.1414	-0.0001	8	8
93.5964	93.540	-0.0564	152	1.0567	1.0572	0.0005	4	4
	93.588	-0.0084	244		1.0568	0.0001		4
	93.667	0.0706	316		1.0561	-0.0006		4
102.361	102.305	0.056	440	0.9887	0.9890	0.0003	2	2
102.536	102.564	0.028	008	0.9875	0.9872	-0.0003	2	1

for Sr₃Fe₂TeO₉, Sr₃Fe₂MoO₉, Sr₃Fe₂ReO₉, and Sr₃Fe₂UO₉ magnetic compounds. Hence, the antisite-disorder which is independent of bond length distortion can be controlled by calculating the relative deviation (relative distortion) from average bond length of the polyhedra Δ_{oct} given by Fleet (1976)

$$\Delta_{\text{oct}} = \frac{1}{6} \sum_{i=1}^n [(l_i - l_0)/l_0]^2.$$

where l_0 is the theoretical bond length calculated from the ionic radii taken from Shannon tables (Shannon, 1976), and l_i is the bond length obtained from the Rietveld refinement (see Table III). The relative distortion of (Sr/Ca)_{4d}O₁₂-polyhedra, (Fe/W)_{2a}O₆ and (Fe/W)_{2b}O₆-octahedra, are illustrated in Table VI. Also, the relative deviation for Sr₃Fe₂WO₉ and Sr₃Fe₂TeO₉ are given for comparison.

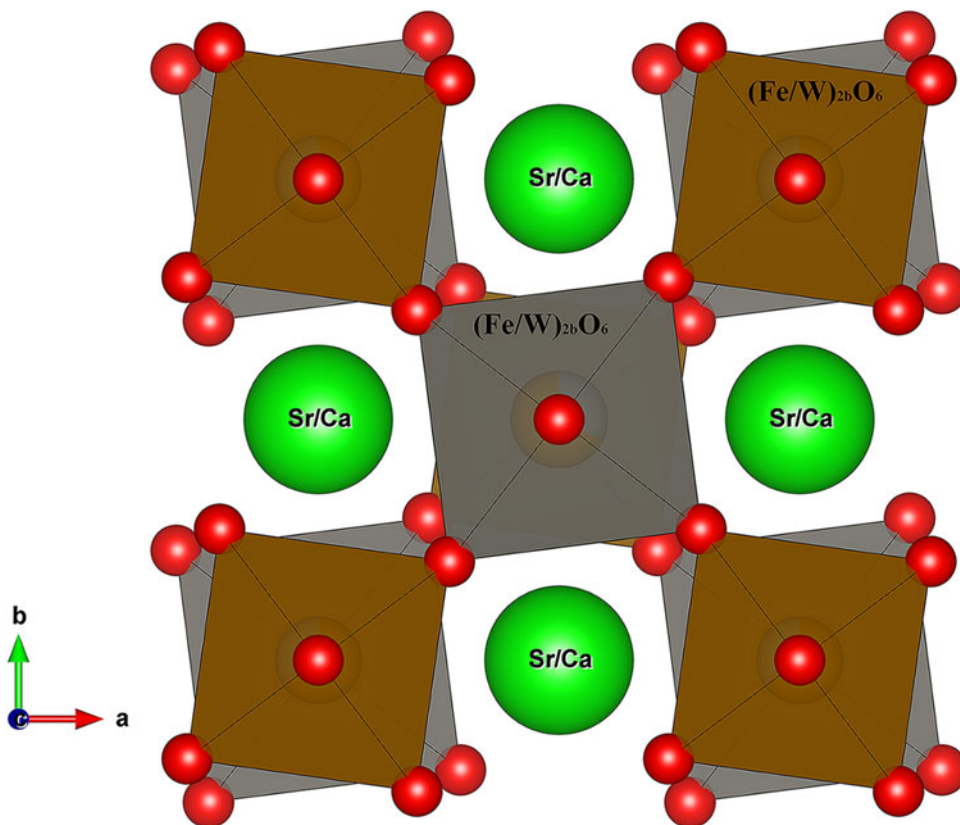


Figure 4. (Colour online) Illustrations of the tilting effect of the $(\text{Fe}/\text{W})\text{O}_6$ octahedra in the tetragonal structure $\text{Sr}_2\text{CaFe}_2\text{WO}_9$. The octahedra are tilted in anti-phase around vertical $[0\ 0\ 1]$ axis (Glazer notation, $a^0a^0c^-$). The Fe and W cations are located inside the $(\text{Fe}/\text{W})_{2a}\text{O}_6$ octahedra and $(\text{Fe}/\text{W})_{2b}\text{O}_6$ octahedra.

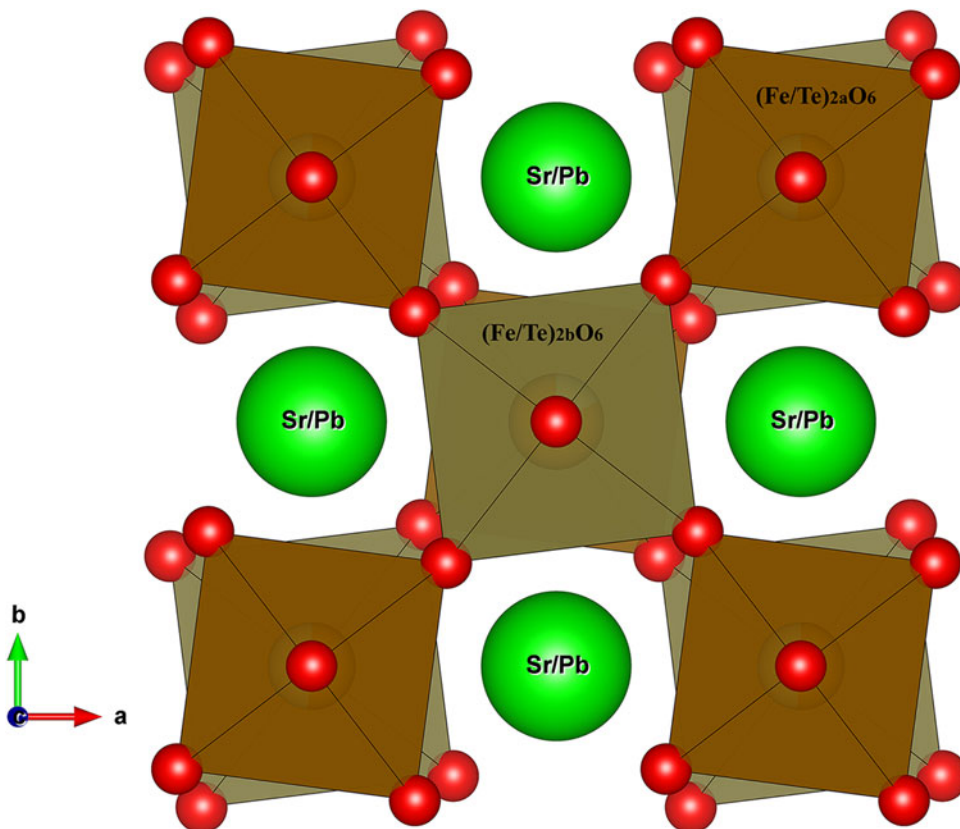


Figure 5. (Colour online) Illustrations of the tilting effect of the $(\text{Fe}/\text{Te})\text{O}_6$ octahedra in the tetragonal structure $\text{Sr}_2\text{PbFe}_2\text{TeO}_9$. The octahedra are tilted in anti-phase around vertical $[0\ 0\ 1]$ axis (Glazer notation, $a^0a^0c^-$). The Fe and Te cations are located inside the $(\text{Fe}/\text{Te})_{2a}\text{O}_6$ octahedra and $(\text{Fe}/\text{Te})_{2b}\text{O}_6$ octahedra.

TABLE VI. Calculated relative deviation from average bond length of the polyhedra of Sr₂CaFe₂WO₉, Sr₂PbFe₂TeO₉, Sr₃Fe₂WO₉, and Sr₃Fe₂TeO₉.

	Δ_{oct} (in 2a site)	Δ_{oct} (in 2b site)	Δ_{poly} (in 4d site)
Sr ₂ CaFe ₂ WO ₉	7.73×10^{-4}	15.8×10^{-4}	31.7×10^{-4}
Sr ₂ PbFe ₂ TeO ₉	14.1×10^{-4}	1.75×10^{-4}	30.1×10^{-4}
Sr ₃ Fe ₂ WO ₉ ^a	13.3×10^{-4}	4.62×10^{-4}	15.9×10^{-4}
Sr ₃ Fe ₂ TeO ₉ ^a	2.51×10^{-4}	17.1×10^{-4}	22.5×10^{-4}

^aCrystallographic information of Sr₃Fe₂WO₉ and Sr₃Fe₂TeO₉ are taken from refs (Ivanov *et al.*, 2001) and (Ivanov *et al.*, 2007) for comparison.

IV. CONCLUSION

In this paper, using XRPD technique, we reported on the crystal structure of Sr₂CaFe₂WO₉ and Sr₂PbFe₂TeO₉ double perovskite oxides. The tetragonal system with space group *I4/m* was adopted for both compounds. The lattice parameters and volumes were different; this is due to larger size of Pb²⁺ compared with that of Ca²⁺. The Fe and W and/or Te cations are partially disordered over the B-sites, indicating the presence of a partial amount of W and/or Te at Fe positions and vice versa.

SUPPLEMENTARY MATERIAL

The supplementary material for this article can be found at <https://doi.org/10.1017/S0885715618000222>

Acknowledgements

The authors are grateful to the Office Chérifien des Phosphates in the Moroccan Kingdom (OCP group) and Mohammed VI Polytechnic University, the University Hassan 1st for its support and the Swedish Research Council for the financial grant SRL(MENA) # 348- 2014-4287.

Arulraj, A., Ramesha, K., Gopalakrishnan, J., and Rao, C. N. R. N. R. (2000). "Magnetoresistance in the double perovskite Sr₂CrMoO₆," *J. Solid State Chem.* **155**(1), 233–237.

Baum, L. A., Stewart, S. J., Mercader, R. C., and Grenèche, J. M. (2004). "Magnetic response and hyperfine magnetic fields at Fe sites of Sr₃Fe₂MO₉ (M=Mo, Te, W, U)," *Hyperfine Interact.* **156/157**(1–4), 157–163.

Boultif, A., Loueër, D., and Louër, D. (1991). "Indexing of powder diffraction patterns for low-symmetry lattices by the successive dichotomy method," *J. Appl. Crystallogr.* **24**(6), 987–993.

Branford, W. R., Clowes, S. K., Bugoslavsky, Y. V., Miyoshi, Y., Cohen, L. F., Berenov, A. V., MacManus-Driscoll, J. L., Rager, J., and Roy, S. B. (2003). "Effect of chemical substitution on the electronic properties of highly aligned thin films of Sr_{2-x}A_xFeMoO₆ (A=Ca, Ba, La; x=0, 0.1)," *J. Appl. Phys.* **94**(7), 4714–4716.

Dass, R. I. and Goodenough, J. B. (2001). "Itinerant to localized electronic transition in Sr₂FeMo_{1-x}W_xO₆," *Phys. Rev. B* **63**(6), 64417.

Dhahri, A., Dhahri, J., and Oumezzine, M. (2009). "Magnetic and electrical properties of Ba₂CrMo_{1-x}W_xO₆ double perovskite," *Mater. Lett.* **63**(1), 121–123.

El Hachmi, A., Manoun, B., Tamraoui, Y., Mirinioui, F., Abkar, R., El aamrani, M. A., Saadoune, I., Sajjedine, M., and Lazor, P. (2017). "Temperature induced structural phase transition in Sr_{3-x}CaxFe₂TeO₉ (0 ≤ x ≤ 1) probed by Raman and Mossbauer techniques," *J. Mol. Struct.* **1141**, 484–494.

Fleet, M. E. (1976). "Distortion parameters for coordination polyhedra," *Mineral. Mag.* **40**, 531–533.

Gao, Y., Chang, H., Wu, Q., Wang, H., Pang, Y., Liu, F., Zhu, H., and Yun, Y. (2017). "Optical properties and magnetic properties of antisite-disordered Ni_{1-x}Co_xCr₂O₄ spinels," *Trans. Nonferrous Metals Soc. China* **27**(4), 863–867.

García-Hernández, M., Martínez, J. L., Martínez-Lope, M. J., Casais, M. T., and Alonso, J. A. (2001). "Finding universal correlations between cationic

disorder and low field magnetoresistance in FeMo double perovskite series," *Phys. Rev. Lett.* **86**(11), 2443–2446.

Glazer, A. M. (1975). "Simple ways of determining perovskite structures," *Acta Crystallogr. Sec. A* **31**(6), 756–762.

Gong, S., Chen, P., and Liu, B. G. (2014). "Structural, electronic, and magnetic properties of double perovskite Pb₂CrMO₆ (M=Mo, W and Re) from first-principles investigation," *J. Magnetism Magnetic Mater.* **349**, 74–79.

Ivanov, S. A., Eriksson, S. G., Tellgren, R., and Rundlöf, H. (2001). "Evolution of the atomic and magnetic structure of Sr₃Fe₂WO₉: a temperature dependent neutron powder diffraction study," *Mater. Res. Bull.* **36**(15), 2585–2596.

Ivanov, S. A., Eriksson, S. G., Erikssen, J., Tellgren, R., and Rundlöf, H. (2004). "Nuclear and magnetic structure of Ba₃Fe₂WO₉," *Mater. Res. Bull.*, **39**(4–5), 615–628.

Ivanov, S. A., Eriksson, S. G., Tellgren, R., and Rundlöf, H. (2005). "Structural and magnetic properties of perovskite Ca₃Fe₂WO₉," *J. Solid State Chem.* **178**(12), 3605–3614.

Ivanov, S. A., Nordblad, P., Eriksson, S. G., Tellgren, R., and Rundlöf, H. (2007). "The magnetoelectric perovskite Sr₃Fe₂TeO₉: an insight from magnetic measurements and neutron powder diffraction," *Mater. Res. Bull.* **42**(4), 776–789.

Kawanaka, H., Hase, I., Toyama, S., and Nishihara, Y. (2000). "Iron spin state of double perovskite oxide Sr₂FeWO₆," *Physica B: Condens. Matter* **281–282**, 518–520.

Kobayashi, K. I., Kimura, T., Sawada, H., Terakura, K., and Tokura, Y. (1998). "Room-temperature magnetoresistance in an oxide material with an ordered double-perovskite structure," *Nature* **395**(6703), 677–680.

Manoun, B., Benmokhtar, S., Bih, L., Azrou, M., Ezzahi, A., Ider, A., Azdouz, M., Annersten, H., and Lazor, P. (2011). "Synthesis, structure, and high temperature Mössbauer and Raman spectroscopy studies of Ba_{1.6}Sr_{1.4}Fe₂WO₉ double perovskite," *J. Alloys Compounds* **509**(1), 66–71.

Philipp, J. B., Majewski, P., Alff, L., Erb, A., Gross, R., Graf, T., Brandt, M. S., Simon, J., Walther, T., Mader, W., Topwal, D., and Sarma, D. D. (2003). "Structural and doping effects in the half-metallic double perovskite A₂CrWO₆ (A=Sr, Ba, and Ca)," *Phys. Rev. B* **68**(14), 144431.

Pinacca, R. M., Viola, M. C., Alonso, J. A., Pedregosa, J. C., and Carbonio, R. E. (2005). "On the new ferrimagnetic Sr₃Fe₂UO₉ double perovskite with T-c above room temperature: a neutron diffraction study," *J. Mater. Chem.* **15**(43), 4648–4653.

Ray, S., Kumar, A., Majumdar, S., Sampathkumaran, E. V., and Sarma, D. D. (2001). "Transport and magnetic properties of Sr₂FeMo_xW_{1-x}O₆," *J. Phys., Condens. Matter.* **13**(4), 607–616.

Rietveld, H. M. (1969). "A profile refinement method for nuclear and magnetic structures," *J. Appl. Crystallogr.* **2**(2), 65–71.

Rodríguez-Carvajal, J. (1990). "Powder diffraction," in *Satellite meeting of the 15th congress of IUCr, Toulouse, France*, p. 127.

Roissel, T., and Rodríguez-Carvajal, J. (2001). WinPLOTR: "A windows tool for powder diffraction pattern analysis," *Mater. Sci. Forum* **378–381**, 118–123.

Sánchez, D., Alonso, J. A., García-Hernández, M., Martínez-Lope, M. J., Martínez, J. L., and Mellergård, A. (2002). "Origin of neutron magnetic scattering in antisite-disordered S₂FeMoO₆ double perovskites," *Phys. Rev. B – Condens. Matter Mat. Phys.* **65**(10), 1044261–1044268.

Shannon, R. D. (1976). "Revised effective ionic radii and systematic studies of interatomic distances in halides and chalcogenides," *Acta Crystallogr. Section A* **32**(5), 751–767.

Sher, F. and Attfield, J. P. (2006). "Synthesis, structure and magnetic properties of Ba₂CrMoO₆," *Solid State Sci.* **8**(3–4), 277–279.

Tang, Y., Hunter, E. C., Battle, P. D., Sena, R. P., Hadermann, J., Avdeev, M., and Cadogan, J. M. (2016). "Structural chemistry and magnetic properties of the perovskite Sr₃Fe₂TeO₉," *J. Solid State Chem.* **242**, 86–95.

Viola, M. D. C., Augsburg, M. S., Pinacca, R. M., Pedregosa, J. C., Carbonio, R. E., and Mercader, R. C. (2003). "Order-disorder at Fe sites in SrFe_{2/3}^{1/3}O₃ (B' = Mo, W, Te, U) tetragonal double perovskites," *J. Solid State Chem.* **175**(2), 252–257.

Viola, M. C., Alonso, J. A., Pedregosa, J. C., and Carbonio, R. E. (2005). "Crystal structure and magnetism of the double perovskite Sr₃Fe₂MoO₉: a neutron diffraction study," *Eur. J. Inorg. Chem.* (2005) (8), 1559–1564.

Woodward, P. M. (1997). "Octahedral tilting in perovskites. II. Structure stabilizing forces," *Acta Crystallogr. B* **53**(1), 44–66.

Woodward, P., Hoffmann, R.-D., and Sleight, A. W. (1994). "Order-disorder in A₂M₃M₅O₆ perovskites," *J. Mat. Res.* **9**(8), 2118–2127.